Influence of upper ocean stratification interannual variability on tropical cyclones

Emmanuel M. Vincent, Kerry A. Emanuel, Matthieu Lengaigne, Jérôme Vialard, Gurvan Madec

AGU PUBLICATIONS

Journal of Advances in Modeling Earth Systems

RESEARCH ARTICLE
10.1002/2014MS000327

Influence of upper ocean stratification interannual variability on tropical cyclones

Emmanuel M. Vincent[1], Kerry A. Emanuel[1], Matthieu Lengaigne[2,3], Jérôme Vialard[2], and Gurvan Madec[2]

[1]Program in Atmospheres, Oceans and Climate, Department of Earth, Atmospheric, and Planetary Sciences, Massachusetts Institute of Technology, Cambridge, Massachusetts, USA, [2]Sorbonne Universités (UPMC, Univ Paris 06)-CNRS-IRD-MNHN, LOCEAN Laboratory, IPSL, Paris, France, [3]Indo-French Cell for Water Sciences, IISc-NIO-IITM-IRD Joint International Laboratory, NIO, Dona Paula, Goa, India

Key Points:
- Downscaling method is used to test ocean variability influence on Hurricanes
- Ocean subsurface temperature significantly influences intense Hurricane frequency

Correspondence to:
E. M. Vincent,
evincent@mit.edu

Citation:
Vincent, E. M., K. A. Emanuel, M. Lengaigne, J. Vialard, and G. Madec (2014), Influence of upper ocean stratification interannual variability on tropical cyclones, *J. Adv. Model. Earth Syst.*, *6*, 680–699, doi:10.1002/2014MS000327.

Received 31 MAR 2014
Accepted 2 MAY 2014
Accepted article online 10 MAY 2014
Published online 5 AUG 2014

Abstract Climate modes, such as the El Niño Southern Oscillation (ENSO), influence Tropical Cyclones (TCs) interannual activity through their effect on large-scale atmospheric environment. These climate modes also induce interannual variations of subsurface oceanic stratification, which may also influence TCs. Changes in oceanic stratification indeed modulate the amplitude of TCs-induced cooling, and hence the negative feedback of air-sea interactions on the TC intensity. Here we use a dynamical downscaling approach that couples an axisymmetric TC model to a simple ocean model to quantify this interannual oceanic control on TC activity. We perform twin experiments with contrasted oceanic stratifications representative of interannual variability in each TC-prone region. While subsurface oceanic variations do not significantly affect the number of moderate (Category 3 or less) TCs, they do induce a 30% change of Category 5 TC-days globally, and a 70% change for TCs exceeding 85 m s^{-1}. TCs in the western Pacific and the southwestern Indian Ocean are most sensitive to oceanic interannual variability (with a ~10 m s^{-1} modulation of the intensity of strongest storms at low latitude), owing to large upper ocean variations in response to ENSO. These results imply that a representation of ocean stratification variability should benefit operational forecasts of intense TCs and the understanding of their climatic variability.

1. Introduction

Tropical cyclone (TC) activity (a term encompassing their location, number, duration, and intensity) displays large year-to-year fluctuations. While part of this variability can be attributed to purely stochastic processes [*Zhao et al*., 2009; *Jourdain et al*., 2011], tropical modes of climate variability such as the El Niño/Southern Oscillation (ENSO) also exert a strong control on TC activity by modulating the large-scale dynamic and thermodynamic environment in which TCs form and develop [e.g., *Chu*, 2004; *Emanuel et al*., 2004; *Vincent et al*., 2011]. Modifications of tropospheric temperature and vertical wind shear related to ENSO teleconnections indeed clearly influence TC frequency in the Atlantic basin [*Tang and Neelin*, 2004] while ENSO-related changes in midtropospheric humidity and large-scale low-level vorticity influence TC activity in the West Pacific basin [*Menkes et al*., 2011; *Vincent et al*., 2011].

The response of TC activity to changes in large-scale atmospheric environment related to tropical modes of climate variability has therefore received much attention [e.g., *Chu*, 2004]. These coupled climate modes, however, also induce oceanic changes that may influence TC activity. The influence of sea surface temperature (SST) variability has, for example, abundantly been discussed [e.g., *Vecchi et al*., 2008]. As TCs draw most of their energy from surface sea-air enthalpy fluxes [*Emanuel*, 1986], background SST along the TC trajectory indeed strongly influences the maximum potential intensity (PI) [*Emanuel*, 1999] of the cyclone. Subsurface oceanic properties could, however, also influence TC intensity. TCs indeed drive intense upper ocean vertical mixing that results in a strong surface cooling along the TC trajectory [*Price*, 1981]. This cooling, or "cold wake," exerts a negative feedback on TC intensity by decreasing sea-air enthalpy fluxes under the storm [*Cione and Uhlhorn*, 2003; *Schade and Emanuel*, 1999]. The amplitude of this cold wake is not only set by the cyclone intensity but also by the characteristics of the oceanic subsurface stratification [e.g., *Jacob and Shay*, 2003; *Lloyd and Vecchi*, 2011; *Vincent et al*., 2012b]. *Vincent et al*. [2012b] indeed demonstrated that the amplitude of the cooling could vary by up to one order of magnitude for a given level of

mechanical energy transfer to the ocean, depending on the ocean characteristics over which the TCs travel. While a large part of the upper ocean stratification variation arises from the geographic contrasts in ocean properties, climate variability also influences oceanic stratification. Ocean stratification variability could hence potentially exert a control on TC activity, in addition to those due to changes in background SST and atmospheric properties.

A few studies [*Balaguru et al*., 2013; *Wada and Chan*, 2008; *Xie et al*., 2002] already acknowledged the potential influence of subsurface ocean temperature variability at climatic time scales on TC activity. TC activity in the northeast [*Balaguru et al*., 2013] and northwest Pacific [*Wada and Chan*, 2008] appears to be correlated to upper layer oceanic properties, such as mixed layer or thermocline depth. Similarly, *Xie et al*. [2002] showed that year-to-year thermocline depth variability in the southwest tropical Indian Ocean was associated with changes in TC activity. Oceanic (e.g., thermocline and mixed layer depth) and atmospheric (e.g., vorticity, shear, moisture...) background characteristics, however, strongly covary under the influence of coupled climate modes such as ENSO [*Vincent*, 2011]. It is thus hard to unambiguously assess the respective influences of atmospheric, SST, and ocean subsurface variability on TC intensity interannual variations from such observation-based analyses.

The aim of the present paper is therefore to quantify the influence of subsurface oceanic variability on TC activity and to disentangle it from atmospheric and SST influences. To that end, we use a dynamical downscaling approach that couples the axisymmetric CHIPS hurricane model [*Emanuel*, 2006; *Emanuel et al*., 2008] to a one-dimensional ocean model accounting for oceanic feedbacks. In this method, TC "seeds" are generated randomly and advected by the mean tropospheric winds. Along their track, the axisymmetric model computes the evolution of the storm intensity resulting from its interactions with its environment [*Emanuel et al*., 2004]. This cost-effective numerical strategy allows us to simulate a large number of TCs at global scale with the full range of TC intensity, while more numerically expensive climate models have a resolution that is too coarse to simulate the most intense TCs.

The paper is organized as follows. Section 2 provides a description of the atmospheric and oceanic components of the coupled downscaling TC model. Section 3 discusses the interannual variability of upper ocean stratification in each tropical oceanic basin and our modeling strategy to assess the influence of these upper ocean interannual variations on TCs. In section 4, we describe how upper ocean stratification influences TCs by modulating the TC-induced cold wake, which then relates to TC intensification rate. Section 5 discusses the year-to-year modulation of TC characteristics by interannual variations of upper ocean stratification. The strongest TCs have the largest societal impact [*Pielke and Landsea*, 1998] and appear to be most sensitive to upper ocean stratification conditions [*Lin et al*., 2008; *Emanuel et al*., 2004]. Section 5 will hence provide a focus on the strongest TCs, which are well sampled by our modeling methodology. Conclusions and perspectives are provided in section 6.

2. Coupled Downscaling TC Model

2.1. Atmospheric Component

We use the method developed by *Emanuel* [2006] and improved by *Emanuel et al*. [2008]. The method is designed to simulate a large number of synthetic TCs and evaluate how they are influenced by climate variations. The realism of the simulated genesis locations, tracks, and TC intensity distribution produced by this model has been assessed in *Emanuel et al*. [2006, 2008]. *Emanuel et al*. [2008] show that this model setup has skill in simulating the seasonal and interannual variability of TC activity. We provide a brief overview of this model here. The reader is referred to *Emanuel et al*. [2006] and their online supplement for further details.

TCs are initiated by inserting warm-core cyclonic vortices with peak wind speeds of 12 m s^{-1} in the model. These "seeds" are randomly distributed in space and time, regardless of SST, season, and latitude, except equatorward of 2° latitude where TCs are not allowed to form. Once a storm is generated, it is advected according to a weighted average of the tropospheric environmental winds between 850 and 250 hPa, plus a beta-drift correction [*Emanuel et al*., 2006]. Storm intensities are computed by running the Coupled Hurricane Intensity Prediction System (CHIPS) model [*Emanuel et al*., 2004] along these tracks. CHIPS is an axisymmetric atmospheric model, formulated in potential radius coordinates, that yields high resolution (of the order of 1 km) in the eyewall of the storm. The evolution of the storm intensity is calculated based on

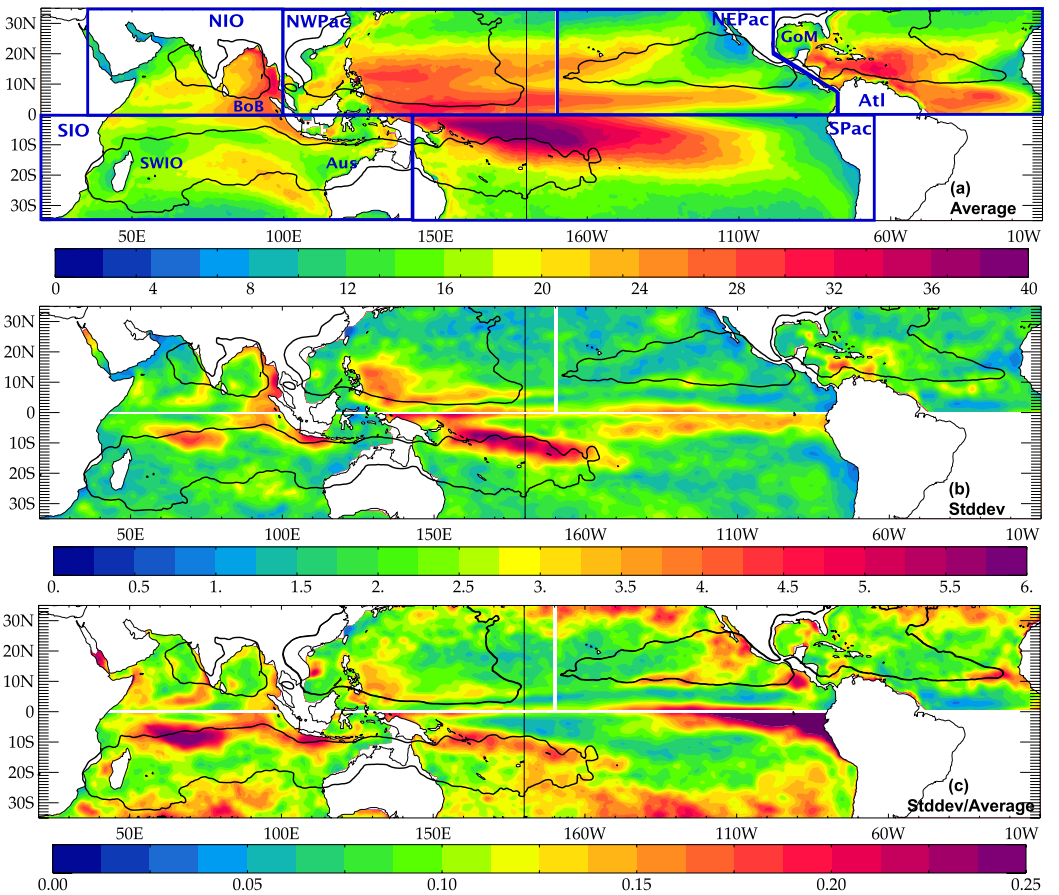

Figure 1. (a) Mean, (b) standard deviation, and (c) normalized standard deviation (standard deviation over mean) of Cooling Inhibition (CI) (in $(J\ m^{-2})^{1/3}$) from GLORYS2 reanalysis over TC-season months in each basin. Regions of usual TC activity are highlighted by the isocontour of 1 TC per 10 years (black contour). Seasonal cycle and linear trend are filtered out of the CI fields before calculating the standard deviation.

enthalpy fluxes from the ocean to the atmosphere. The CHIPS model also uses a parameterization of the deleterious effect of environmental wind shear on tropical cyclones, developed empirically so that the model's real-time predictions match observed storm intensities [see *Emanuel et al.*, 2006]. If the predicted maximum wind drops below 13 m s^{-1}, the storm is assumed to have dissipated and the integration is discontinued. A seed is considered to evolve into a TC if its 1 min sustained winds exceed 21 m s^{-1}. The vast majority of seeds fail to develop into TCs and rapidly decay after initiation, succumbing due to small potential intensity (PI), large wind shear, or low midtropospheric entropy they encounter along their tracks.

In the present study, we perform separate simulations for each of the six major TC-prone basins (Figure 1a), namely, the north Indian Ocean (NIO; 40°E–105°E), the north-west Pacific basin (NWPac; 105°E–170°W), the north-east Pacific (NEPac; east of 170°W), the north Atlantic basin (Atl), the south Indian Ocean (SIO; 30°E–143°E), and the south Pacific basin (SPac; east of 143° longitude). TC characteristics are only studied during the peak TC-season of each basin, i.e., May to June and October to November for the NIO, August to October in the NWPac and Atl, July to September in the NEPac, and January to March in the SIO and SPac. TC track observations are from the Joint Typhoon Warning Center (JTWC) database. The Saffir-Simpson scale is used to bin TCs into categories of increasing intensity. Tropical depressions with winds greater than 18 m s^{-1} are classified as Tropical storms (TSs). Tropical cyclones belong to Category 1, 2, 3, 4, or 5 if their maximum wind reaches 33, 43, 49, 58, or 70 m s^{-1}, respectively. Results for the most intense TCs are detailed by dividing Category 5 TCs into two subcategories: Category 5a (5b) includes Category 5 TCs with maximum winds weaker (greater) than 85 m s^{-1}.

2.2. Oceanic Component

To account for oceanic feedbacks due to SST cooling under the TC track, this axisymmetric hurricane model is coupled to a one-dimensional ocean model (described in detail in *Emanuel et al*. [2004]). The initial state of the ocean is described using four quantities: sea surface temperature (SST), mixed layer depth (h), the temperature jump at the base of the mixed layer ΔT, and the temperature lapse rate below the mixed layer (Γ). The mixed layer is initially at rest and horizontal velocity (u) is driven by surface wind stress (τ_S) as $\partial_t \rho h u = |\tau_S|$, where ρ is the seawater density. In the following, we compute seawater density based on temperature only as the variability of upper ocean stratification related to salinity is of second order on interannual time scales (see section 3.2). The mixed layer depth evolution is calculated based on the assumed constancy of a bulk Richardson number, $Ri = (g\alpha\Delta T h)/u^2$, where g is the acceleration of gravity and α is the coefficient of thermal expansion of seawater. If the Richardson number falls below a threshold of 1, cold water is entrained from below into the mixed layer. The ML depth is increased accordingly and its temperature is calculated assuming heat conservation. A set of these one-dimensional ocean models is used along the TC track to calculate the TC-induced SST cooling and its feedback on enthalpy fluxes to the atmosphere. While this simple framework does not represent the SST evolution in the days following the storm passage properly (inertial oscillations have a strong influence on mixing) [e.g., *Price*, 1981], it captures most of the processes controlling the SST variations under the eyewall, to which the TC model is mostly sensitive.

3. Interannual Variability of Upper Ocean Stratification and Experimental Strategy

3.1. Ocean Data

The interannual variability of upper ocean parameters used to force the oceanic model described in section 2.2 are derived from the GLORYS2 ocean reanalysis [*Ferry et al*., 2012; *Jourdain et al*., 2013, 2014]. GLORYS2 spans the 1993–2009 period corresponding to the availability of satellite altimetry. It uses the NEMO (Nucleus for European Modelling of the Ocean) [*Madec*, 2008] global ocean model at 1/4° horizontal resolution with 75 vertical levels (and a stretched grid comprising 22 levels in the upper 100 m). GLORYS2 assimilates both altimetry and in situ observations, and its temperature and salinity fields agree favorably with observations, especially within the first 300 m [*Ferry et al*., 2012], where ocean characteristics matter most for TCs. The accurate representation of interannual variability of surface height anomalies [*Ferry et al*., 2012] also indicates that the reanalysis properly captures the inner-ocean interannual thermohaline variability. The ocean reanalysis is used to infer the main mode of interannual variability of the subsurface ocean stratification (section 3.2) and to estimate values of the oceanic variables (mixed layer depth, temperature jump at the bottom of the mixed layer, and temperature lapse rate in the thermocline) used in the ocean component (section 3.3). In the following, "interannual" anomalies are derived by removing (i) the seasonal cycle (as a best fit of the first three harmonics) and (ii) a linear trend over the 1993–2009 period at each location (grid point).

3.2. Interannual Upper Ocean Fluctuations

To measure the influence of subsurface ocean properties on the amplitude of TC cold wakes, we use the Cooling Inhibition index (CI) [*Vincent et al*., 2012b]. CI measures the amount of potential energy required to trigger a given surface cooling through vertical mixing, the main process responsible for cooling under TCs [*Price*, 1981; *Vincent et al*., 2012a]. In the present study, this cooling is taken to be 1°C and CI is therefore calculated as follows:

$$CI = [\Delta E_p(-1^\circ C)]^{1/3} \text{ with } \Delta E_p(\Delta T) = \int_{h_m(\Delta T)}^{0} (\rho_f(\Delta T) - \rho_i(z)) g z dz \quad (1)$$

where ρ_i is the initial unperturbed density profile, g is the acceleration of gravity, z is ocean depth, ρ_f is the final density profile (considered to be homogeneous down to the depth h_m), and h_m is the mixing depth necessary to produce a ΔT surface cooling via vertical mixing, assuming heat conservation. CI captures the resistance of the ocean to surface cooling via vertical mixing. It is mostly controlled by two parameters: the initial mixed layer depth (MLD) and the strength of the subsurface stratification (as can be shown by a regression analysis of these parameters to CI). The deeper the initial mixed layer, the more water has to be entrained to decrease SST by 1°C. High thermal stratification at the base of the mixed layer ($\Gamma = dT/dz$)

both stabilizes the water column and allows cooler water to be entrained into the ML. The later effect is usually dominant, with a higher thermal stratification resulting in a stronger surface cooling. As discussed by *Vincent et al*. [2012b] and *Neetu et al*. [2012], CI is a physically based variable that accurately captures the inhibition of mixing-induced surface cooling by the ocean background state. For a given cyclone, a low CI can result in a surface cooling that is up to one order of magnitude stronger than a high CI [*Vincent et al*., 2012b].

Figure 1a displays a climatological map of CI averaged over the TC-season for each basin considered here. Highest CI values in TC-prone regions are found in the equatorial West Pacific (the warm pool), the eastern part of the Bay of Bengal (BoB) and in the Caribbean Sea, at the exit region of the Atlantic Main Development Region. As a stable upper ocean stratification translates into high CI values, the ocean cooling induced by TCs in these regions is therefore expected to be weak and favorable to TC intensification [e.g., *Balaguru et al*., 2012]. Lowest CI values in TC-prone regions are found in the northeast Pacific, in the Thermocline Ridge of the Indian Ocean region (TRIO) [*Vialard et al*., 2009] and in the Gulf of Mexico (GoM). Surface cooling under TCs in these regions is therefore expected to be large, hence less favorable to the development of intense TCs.

The variability around this climatological picture is first evaluated by displaying CI standard deviation at interannual time scales (Figure 1b) along with CI standard deviation normalized by its mean value (Figure 1c). The northern end of the South Pacific (SPac) region (along a line from the Solomon Islands to Samoa where numerous TCs form) displays the largest CI variability. CI variability is also large off Philippines coasts, along the coasts of the Bay of Bengal (BoB) and in the southwestern Indian Ocean in the TRIO region. This latest region stands out as the TC-prone region with the largest relative CI variability (28%; Figure 1c) due to the relatively low CI climatological values there. Similarly, despite a weaker absolute CI variability (Figure 1b), the coasts of Mexico in the NEPac experience strong relative variations from the climatological CI. In the Atlantic, CI interannual variability is relatively weak.

The spatial patterns of the dominant modes of upper ocean stratification interannual variability are further assessed by performing an Empirical Orthogonal Function analysis (EOF) [*Reyment and Jörekog*, 1993] of monthly CI interannual anomalies during the months of TC-prone season activity in each basin. The EOF calculations are restricted to the regions of TC activity (i.e., within the climatological 0.1 TC yr^{-1} contour) and spatial patterns associated with the first EOF in each basin are displayed in Figure 2. Table 1 shows the percentage of variance explained by the first three modes in each basin: except in the NEPac and Atl regions, the first mode is generally well separated from the second, and hence represents the bulk of large-scale CI variations. The top modes of upper ocean variations are related to climate variability by correlating the time series associated with the first EOF—the first Principal Component (PC)—by basin to the main known modes of coupled variability in the tropics in Table 2.

In the Pacific, largest CI variability amplitude is found at low latitudes with a maximum in the 5–20° band (Figure 2). In the western Pacific (NWPac and SPac), this first mode explains about half of the total interannual variance (Table 1) and much more than the second mode. It is strongly linked to ENSO variations as shown by the −0.9 correlation between the first PC and the Niño 3.4 index for both western Pacific regions (Table 2). During an El Niño (La Niña), westerly (easterly) wind anomalies in the central Pacific force westward propagating Rossby waves that lift (deepen) the thermocline in the western Pacific [e.g., *Boulanger and Menkes*, 1995]. Although weaker, this correlation with ENSO is still significant in the Northeast Pacific (0.6) and may be related to fluctuations of the Intertropical Convergence Zone and associated Ekman pumping. The variance explained by the first mode in the NEPac is, however, smaller (18%) and close to the one explained by the second mode.

In the Indian Ocean (NIO and SIO), the first CI mode explains more than a third of the total variance and exhibits largest variations in the TRIO region, along the Java/Sumatra coast and along the eastern flank of the Bay of Bengal. This mode is related to both the Indian Ocean Dipole (IOD) [*Saji et al*., 1999; *Webster et al*., 1999] and ENSO variability (Table 2). These two climate modes are indeed associated with wind fluctuations in the central Indian Ocean that force Kelvin waves and drive interannual thermocline fluctuations along the coast of Sumatra and the Bay of Bengal [*Aparna et al*., 2012]. Similarly, both IOD and ENSO induce anticyclonic winds south of the equator that drive thermocline variations in the TRIO region [e.g., *Yu et al*., 2005; *Tozuka et al*., 2010].

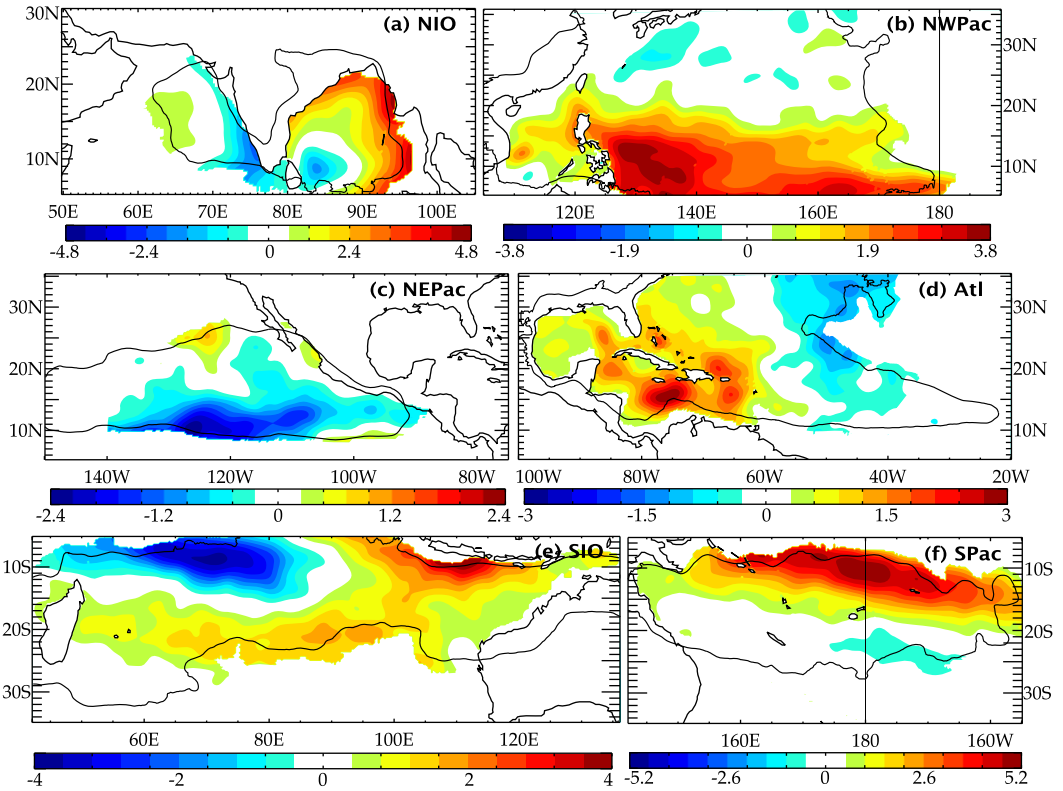

Figure 2. First EOFs of CI by basin: (a) NIO, (b) NWPac, (c) NEPac, (d) Atl, (e) SIO, and (f) SPac. Associated PCs have been normalized to have a standard deviation of 1, so that these maps contain information on the magnitude of CI variability. The EOF analyses have been restricted to the regions of TC activity (i.e., within the climatological 0.1 TC yr^{-1} contour). Note the different color scale for each panel.

Finally, the first mode in the Atlantic is dominated by CI variability in the Caribbean Sea but does not relate to ENSO variability or to the "Atlantic El Niño" [*Deser et al*., 2010]. The first PC is weakly, but significantly, related to the Atlantic Meridional Mode (AMM) [*Chiang and Vimont*, 2004], which has already been suggested to influence TC activity in the Atlantic region [*Kossin and Vimont*, 2007].

We note that the contribution of salinity stratification to the total CI variability is of second order as shown by the high similarity of the first EOF of CI and the first EOF of CI calculated holding salinity constant as defined in *Neetu et al*. [2012] (not shown).

3.3. Experimental Strategy

We aim at assessing the influence of these interannual variations of oceanic upper stratification on TC activity. To that end, we perform two experiments with the coupled TC models for each of the six major TC-prone basins described in section 2 (Figure 1a). Thanks to the low computational cost of this model, ~3000 TCs are generated for each major TC basin in each experiment. We run twin experiments, with the atmospheric component using the same interannually varying atmospheric and surface conditions derived from monthly fields of the NCEP reanalysis [*Kalnay et al*., 1996] over the 1980–2009 period while the ocean component uses two time unvarying and contrasting upper oceanic conditions (details below) that are representative of the interannual departures from the mean state described above. Our two sets of experiments use the same sets of tracks and the same atmospheric and sea surface temperature conditions. TC

Table 1. Percentage Variance Explained by the First Three Principal Components (PCs) of Cooling Inhibition (CI) in Each Basin

	NIO (%)	SIO (%)	NWPac (%)	SPac (%)	NEPac (%)	Atl (%)
PC 1	35	34	47	48	18	18
PC 2	12	10	6	11	14	14
PC 3	7	8	5	7	11	8

Table 2. Correlation of Cooling Inhibition (CI) First Principal Component (PC) to Known Modes of Tropical Climate Variability: Indian Ocean Dipole (IOD), Subtropical IOD Mode (Subtrop. IOD), El Niño (Niño 3.4), Atlantic El Niño (Atl. Niño), and Atlantic Meridional Mode (AMM)[a]

	NIO	NWPac	NEPac	Natl	SIO	SPac
IOD	**−0,7**	−0,4	−0,2	0,0	**0,9**(3)	−0,6(3)
Subtrop. IOD	0,4	0,1	0,2	−0,2	**−0,7**	0,4
Niño 3.4	**−0,7**(1)	**−0,9**	**−0,6**	−0,2	**−0,9**(3)	**−0,9**
Atl. Niño	0,0	0,6(5)	0,4	−0,3	**0,7**(11)	−0,6(11)
AMM	0,2	0,0	0,4	**−0,5**	0,4	−0,4

[a]Figures in brackets indicate the lead lag (in month) if the correlation is increased with respect to the no-lag case.

intensities will hence differ only because of modified upper ocean stratification that modulates the amplitude of the cold wake feedback. This simple setup therefore allows us to assess the influence of upper ocean variability on TC intensity independently of any other environmental influence.

The two contrasting upper oceanic conditions used to force the twin experiments in each basin are derived as follows. Three variables are necessary as input to the ocean component of the CHIPS model: MLD, the temperature lapse rate below the ML (Γ), and the temperature jump at the ML base (ΔT). Interannual anomalies of these variables are first computed from monthly GLORYS2 outputs (as explained in section 3.1). These anomalies are then regressed on the PC of the first EOF of CI interannual variations in each basin displayed in Figure 2. Finally, two composites are produced for each variable by averaging the anomaly fields in the 10% highest ("positive") and lowest ("negative") percentile months of the first PC of CI. Contrasting the 10% highest and lowest percentile allows us to assess the first-order influence of upper ocean interannual variability. In the following, we call "positive" ("negative") the experiments corresponding to months that project positively (negatively) on the first EOF of CI in each basin.

"Positive" composites are displayed in Figure 3 for MLD and Γ. "Negative" composites are almost the opposite of "positive" composites (not shown). Similarly, composites for ΔT are not displayed, as this variable has a weaker influence on TC-induced cooling than the two former ones. As discussed earlier, enhanced CI is favored by an anomalously deep MLD and weak thermocline stratification (e.g., in the western Pacific or Eastern Indian Ocean for the "positive" composite).

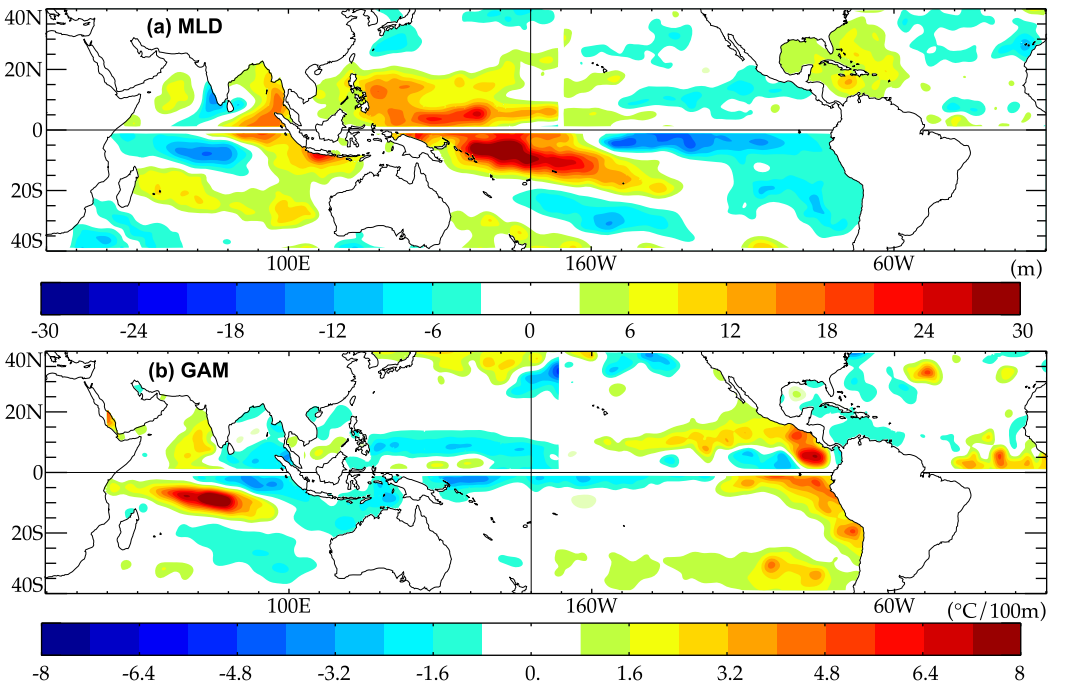

Figure 3. (a) MLD and (b) $\Gamma = dT/dz$ composites of ocean variables anomalies used to alter climatological ocean profiles in the "positive" experiment. Composites for the "negative" experiment are approximately a mirror image of the positive ones.

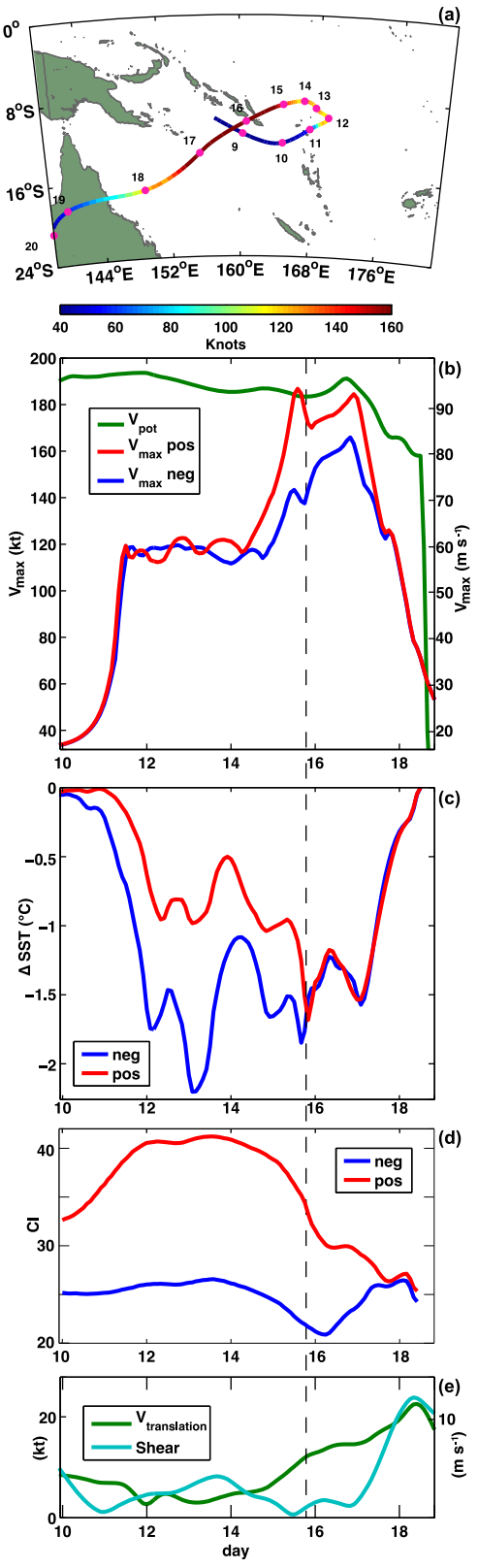

Figure 4. Example of a TC making landfall in the Solomon islands. (a) Map of TC track and intensity (in the "positive" experiment), (b) potential intensity and actual storm intensity, (c) sea surface cooling under the TC-eye, (d) Cooling Inhibition (CI), and (e) translation speed and vertical wind shear in both "positive" and "negative" experiments as a function of time.

In the rest of the paper, we use the term "favorable" ("unfavorable") to refer to conditions where the CI is higher (lower) than climatology at a given ocean location, and hence more favorable (less favorable) to TC intensification. The relative differences between the two experiments discussed below are calculated as ("positive"-"negative")/reference; with the reference taken as the average between "positive" and "negative" simulations.

4. Influence of Ocean Subsurface on TC Intensification

Before discussing how interannual anomalies of upper ocean stratification influence basin-wide TC activity, this section describes the mechanisms by which ocean subsurface variations influence TC intensification through its control of TC-induced surface cooling.

4.1. A Case Study

As a first illustration, we now compare the lifecycle of a TC simulated in the SPac in the two experiments described above (Figure 4). This simulated TC made landfall in the southern Solomon archipelago with a surface wind speed of 90 m s^{-1} in the "positive" experiment (70 m s^{-1} in the "negative" experiment) on day 15–16 (Figures 4a and 4b). At the time of landfall, the environmental vertical wind shear was very low (<2 m s^{-1}; Figure 4e) allowing the storm to reach an intensity close to its maximum potential intensity (PI) (Figure 4b). The TC reached its PI in the "positive" experiment (day 16–17) but not in the "negative" experiment because of a slower intensification rate on day 15–16. This slower intensification rate for the "negative" experiment can be related to the larger surface cooling during the days preceding landfall (Figure 4c). This larger surface cooling was allowed by the lower CI values in the "negative" experiment during this period (Figure 4d).

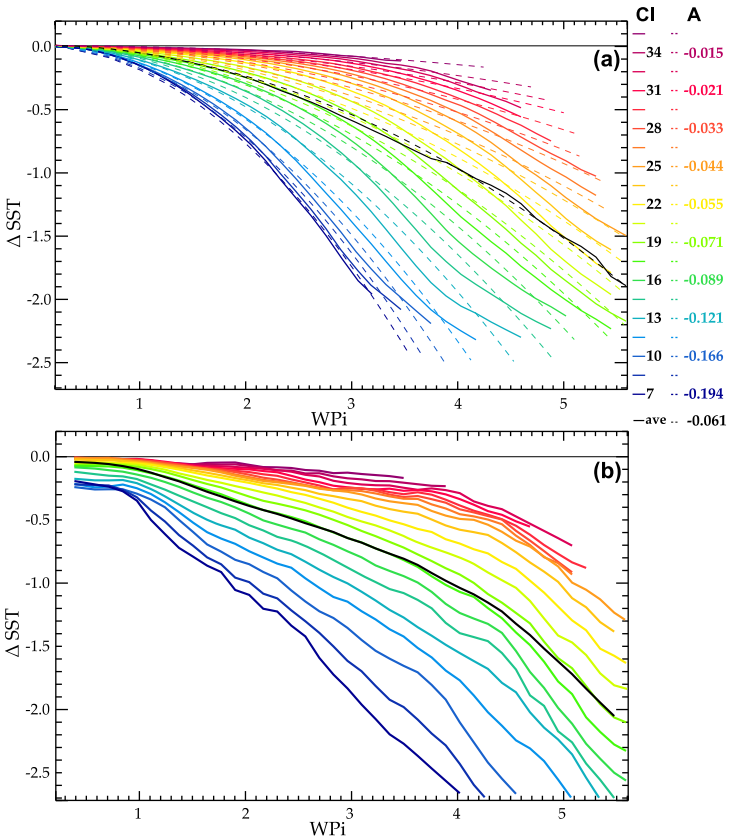

Figure 5. (a) SST cooling under the eyewall as a function of WPi for different values of oceanic Cooling Inhibition (CI) in the "positive" experiment. Dashed lines show the least squares fit between surface cooling magnitude and WPi^2 ($\Delta SST = A\,WPi^2$); values of CI and the corresponding fit coefficients (A) are given on the right. (b) Same diagnostic in the full physics 3-D ocean model NEMO ran at 0.5° resolution (simulation described in *Vincent et al.* [2012a]).

4.2. Influence of Ocean Stratification on TC-Induced Eyewall Cooling

Figure 5 further allows generalizing the relationship between the amplitude of TC-induced cooling and the characteristics of the upper ocean stratification. Following *Vincent et al.* [2012b], we use the Wind Power index (WPi, a scaled version of the Power Dissipation) as a proxy of the mechanical energy deposited by the TC into the ocean. It is the energy deposit that induces vertical mixing, and this quantity is hence relevant to describe the TC-induced surface cooling amplitude [*Vincent et al.*, 2012b]. This dimensionless number is defined as $WPi = [PD/PD_0]^{1/3}$ with $PD = \int_{t_o}^{t_c} \rho_a C_D |\mathbf{V}|^3 dt$, where $|\mathbf{V}|$ is the local magnitude of surface wind, C_D the dimensionless surface drag coefficient, ρ_a is the surface air density, t_0 corresponds to 3 days before the TC reaches the location of interest, and t_c is the time when the TC reaches the location of interest. $PD_0 = \int_{t_o}^{t_c} \rho_a C_D |\mathbf{V}_0|^3 dt$ is a normalization constant corresponding to a typical weak storm with a translation speed of 7 m s^{-1} and maximum 1 min averaged wind speed of 17 m s^{-1} (the wind speed defining a Tropical Depression). WPi is a relevant measure of the TC-induced cooling as it integrates the maximum wind speed in time, allowing one to account for the fact that slower storms transfer more momentum to surface currents and hence trigger more cooling by mixing [e.g., *Mei et al.*, 2012; *Lloyd and Vecchi*, 2011].

As shown in Figure 5a, sea surface cooling magnitude under the TC eyewall increases monotonically with WPi, with surface cooling scaling as $\Delta SST = A\ WPi^2$ in our ocean model (where A is calculated from a least squares fit between surface cooling magnitude and WPi^2 and represents the sensitivity of surface cooling to increasing wind forcing). Upper ocean stratification greatly modulates the surface cooling magnitude as seen from the dependence of the A coefficient on CI, with a CI above 30 resulting in a negligible cooling even for a WPi above 3, while a CI below 15 results in a cooling of 1.5°C or more.

It is difficult to validate the behavior of the cooling seen in Figure 5a against observations. Microwave satellites indeed do not allow one to retrieve SST under heavy precipitation [*Wentz et al*., 2000] and hence do not resolve the cooling under the TC-eye. While microwave satellites do resolve the cooling ~2 days after the cyclone passage, the simple ocean model we use does not account for inertial oscillations and, hence, cannot be used to represent the SST evolution in the aftermath of the cyclone passage. On the other hand, *Vincent et al*. [2012b] used an ocean general circulation model (OGCM) for which the cold wake (SST a few days after the cyclone passage) compares very well to microwave data. We thus use that OGCM in order to validate the relationship between the cooling under the TC-eye and CI and WPi seen in Figure 5a. Despite the simplicity of the 1-D model that only accounts for vertical mixing, sea surface cooling dependence on wind power and ocean stratification compares well (Figure 5b) with the same diagnostic performed using the OGCM simulation from [*Vincent et al*., 2012b]. This gives confidence in the realism of the surface cooling simulated in the present study.

Displaying the spatial pattern of the *A* coefficient allows us to illustrate the importance of spatial variability of upper ocean stratification in controlling hurricane-ocean coupling (Figures 6a and 6b). This coefficient indeed varies by a factor of up to 10 within the TC-prone regions. The sensitivity of surface cooling to wind forcing is largest in the NEPac basin and in the TRIO region, where CI values are particularly low due to a shallow thermocline. In contrast, it is relatively weak in the western Pacific and Caribbean regions, where CI is considerably larger. Figure 6c shows the difference in the value of *A* between the two experiments. Large interannual variations of *A* are observed in the Indian Ocean, western tropical Pacific Ocean, and NEPac region. Figure 6d shows a scatterplot of *A* against CI in both experiments and shows that *A* (the sensitivity of the cooling to WPi) grows as the square root of CI. Figure 6e shows the same scatterplot but of interannual variations of *A* against interannual variations of CI (both estimated from the difference between the two experiments), indicating a roughly linear relation between the two. The impact of the ocean stratification on the cyclone-induced cooling is hence roughly linearly related with interannual anomalies of CI, but weighted by squared WPi, i.e., it will be strongest for the most intense cyclones.

4.3. Influence of TC-Induced Eyewall Cooling on TC Intensification Rate

The amplitude of TC-induced cooling further strongly modulates TC intensification rates (Figure 7). On average, TC intensification rates decrease almost linearly with the surface cooling magnitude, with TCs generally intensifying for cooling weaker than 1°C and decaying for larger cooling. The sensitivity of TC intensification rates to eyewall surface cooling is ~4 (m s^{-1} d^{-1})/°C, a rate that compares qualitatively well with observation-based estimates by *Mei et al*. [2012, Figure 2]. From their results, the intensification rate sensitivity to surface cooling is ~4 (m s^{-1} d^{-1})/°C, if we assume that the cooling they used ("maximum negative SST anomaly" in the TC wake) is twice the eyewall cooling, as suggested by *Vincent et al*. [2012a, Figure 11]. In agreement with *Mei et al*. [2012], we also find that this sensitivity does not depend on TC intensity (not shown).

5. Interannual Modulation of TCs Statistics by Oceanic Stratification

The previous section illustrates how upper ocean stratification variability controls the amplitude of TC-induced surface cooling, which in turn modulates TC intensification. In this section, we describe the TC activity modulation resulting from interannual variations of upper ocean stratification in each basin by comparing the TC statistics of the "positive" and "negative" experiments.

5.1. Changes in Integrated TC Activity

In the following, we use the power dissipated by TCs at the surface (PD defined in section 4.2) as an integrated measure of TC activity and destructive power [*Emanuel*, 2005].

Figures 8a and 8b show the mean PD (average of the "positive" and "negative" experiments) and the relative PD change between the two experiments, while Table 3 provides spatially integrated PD values in each basin. Figure 8a underlines the familiar regions of TC occurrence. The highest TC activity occurs in the northwest and northeast tropical Pacific. There is also a high PD in the southwestern Indian Ocean, in the Atlantic and North of Australia (both on the Indian Ocean and Pacific sides). The Northern Indian Ocean displays the weakest integrated TC wind power. The strongest influence of oceanic stratification on PD (up to 50%) is found in the southwestern Indian Ocean within the 10°S–15°S latitude band, 5° north of the PD maximum

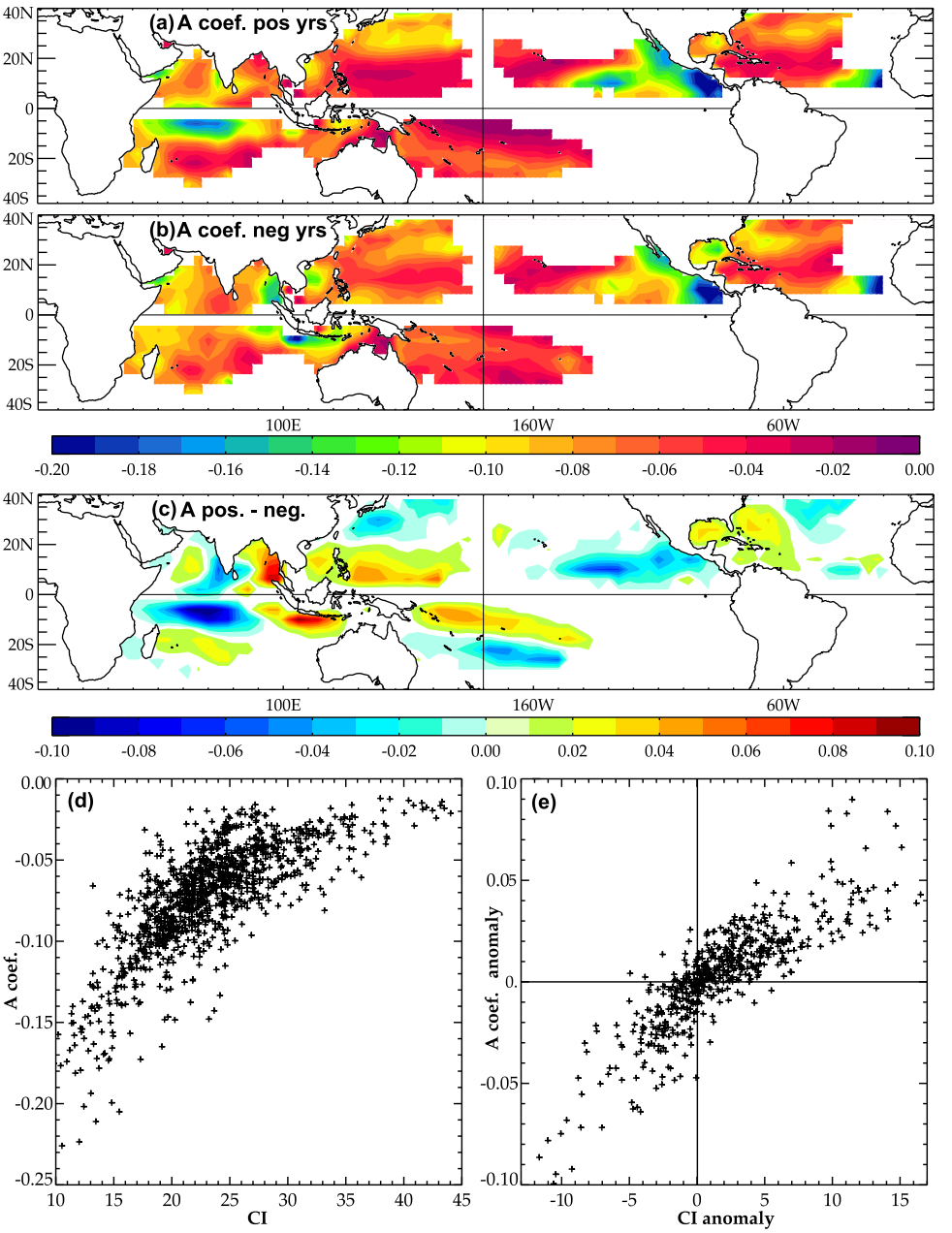

Figure 6. Maps of A (the sensitivity of TC-induced surface cooling evaluated from linear fit: $\Delta SST = A \times WPi^2$) in (a) "positive" experiment, (b) "negative" experiment, and (c) "positive"-"negative" anomaly. (d) Scatterplot of A versus CI at each location (in both experiments) and (e) interannual anomalies of A versus interannual anomalies of CI.

(Figure 8a) and a few degrees south of the strongest CI variability in this basin (Figure 2). When spatially integrated over the basin, this results in an overall 17% reduction of PD in the "positive" simulation with respect to the "negative" one in the SWIO (Table 3). In the Pacific basin, PD is also appreciably altered by ocean stratification with largest relative changes of about 20% between 5° and 10° latitude and basin-integrated differences of about 10%. The "Aus" region displays a similar 10% modification, with the largest changes (locally up to 50%) occurring south of the Java coastline. PD changes are rather weak in the NIO, although the response in the Arabian Sea may not be realistic due to overestimation of TC activity in this region (not shown). The integrated effect of oceanic stratification on PD is also rather weak in the Atlantic basin (Table 3) but changes can be locally large, with about 15% difference in the Gulf of Mexico and between Cuba and Florida.

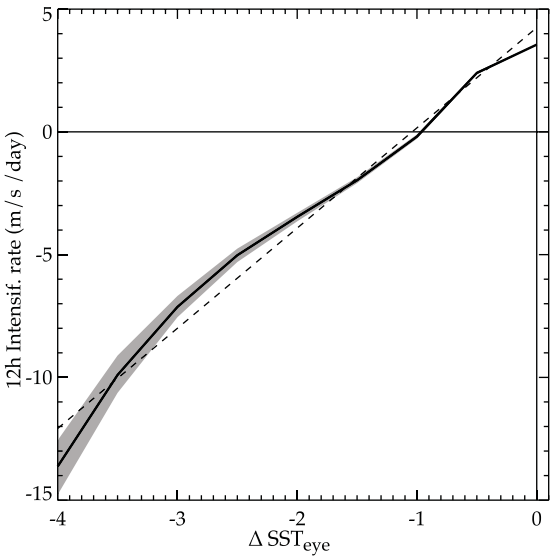

Figure 7. Sensitivity of TCs intensification rate to surface cooling. Thick line is the average intensification rate (between t_0 and t_0 + 12h) as a function of surface cooling under the eyewall (at t_0). Dashed line is the least squares linear fit of this relation and has a slope of 4.1 (m s^{-1} d^{-1})/°C. Shading shows the 90% confidence interval.

These patterns of PD changes can easily be related to the changes of surface cooling sensitivity (*A* coefficient, i.e., the sensitivity of the cooling to WPi; Figure 6c) in response to the contrasted upper ocean stratification used in the two experiments. The similarity between the spatial patterns of Figures 6c and 8b illustrates that the largest changes in PD occur in regions where surface cooling below TCs responds most to changes in ocean stratification. Indeed, large values of *A* yield a strong cooling for a given cyclone energy transfer to the ocean, and hence a stronger negative feedback on the TC intensification rate, as seen in section 4. These results illustrate that interannual upper ocean variability modulates the oceanic feedback on Tropical Cyclones, thereby modifying the integrated TC intensity.

5.2. TC Activity Change as a Function of Intensity

PD anomalies discussed in the previous section provide an integrated view of the influence of oceanic stratification on TCs. Here we further detail this influence as a function of the TCs intensity (Figure 9). The total number of Tropical Storms (TSs) and TCs is hardly modified between the two simulations (less than 1%). Ocean stratification changes mainly act to shift the intensity distribution without deeply influencing the genesis rate, or the storms in their early life stage. Counts of TCs up to Category 3 do not significantly differ

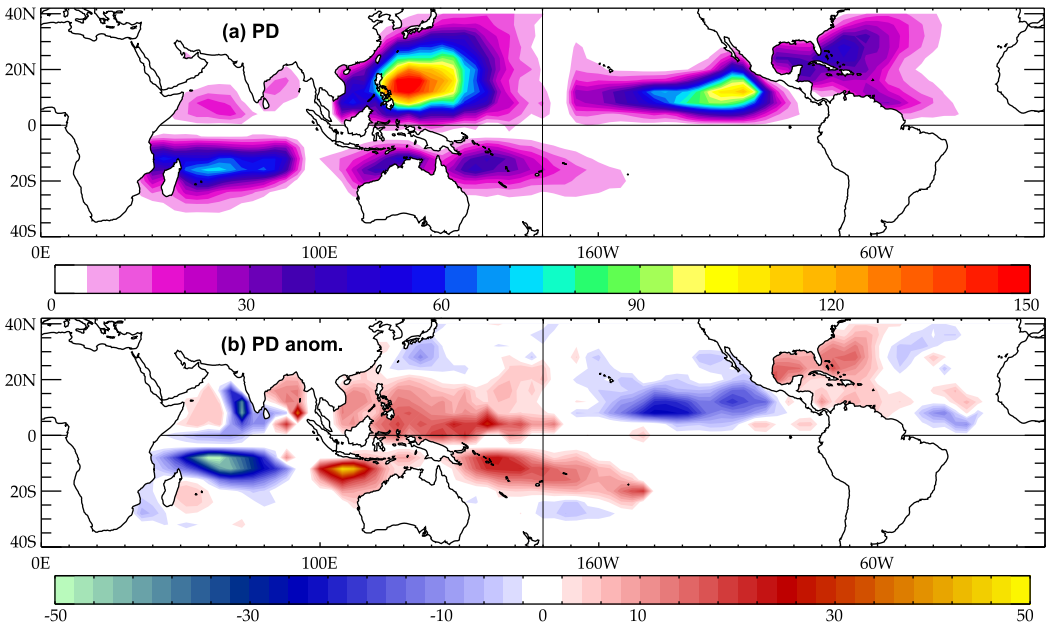

Figure 8. Maps of yearly average power dissipated (in 10^3 m^3/s^3 per year and per 1° lon-lat area). (a) Climatological mean (averaged over the "positive" and "negative" experiments) and (b) relative difference between "positive" and "negative" experiments with respect to mean state (in %).

Table 3. Area Weighted Integrated TC Power Dissipated (PD) by Basin (in 10^{12} m^3/s^3 per year), % of PD Associated With Category 5 TCs, % PD Anomalies in "Positive" Minus "Negative" Experiments (Showing the Influence of Ocean Stratification Variability) and in La Niña Minus El Niño Years (Illustrating the Influence of Atmospheric and SST Variability)

	NIO	NWPac	NEPac	Natl	SWIO	Aus	Spac
PD tot (all TCs)	75	1375	701	410	483	138	202
Cat5 % of tot PD	26	42	17	27	21	42	46
POS-NEG (% diff.)	5	8	−12	7	−17	9	13
Niña-Niño (% diff.)	−14	−26	−57	64	77	12	−14

between the two experiments in any of the basins (Figure 9). The change of TC number per category between the two simulations, however, increases for highest TC categories. TC counts are significantly different in the SWIO and NEPac basins for Category 4 TCs, while they are not significantly altered in other basins. The number of Category 5 TCs is significantly influenced by interannual variability of the oceanic stratification in all basins. Even if they only represent a small fraction of the total number of TCs (∼5%), Category 5 TCs account for an appreciable (∼20–40%) fraction of the total PD depending on the basin (Table 3). The largest modifications in TC Category 5 counts are found in the SWIO and SPac where there is a difference greater than 40% between the "positive" and "negative" simulations (Figure 9). In the NWPac, NEPac, and Atlantic basins, the differences in number of Category 5 TCs reach 27%, 31%, and 20%, respectively. The NIO and Aus basins are the basins where the ocean influences TC Category 5 least, with a ∼15% difference between the two simulations.

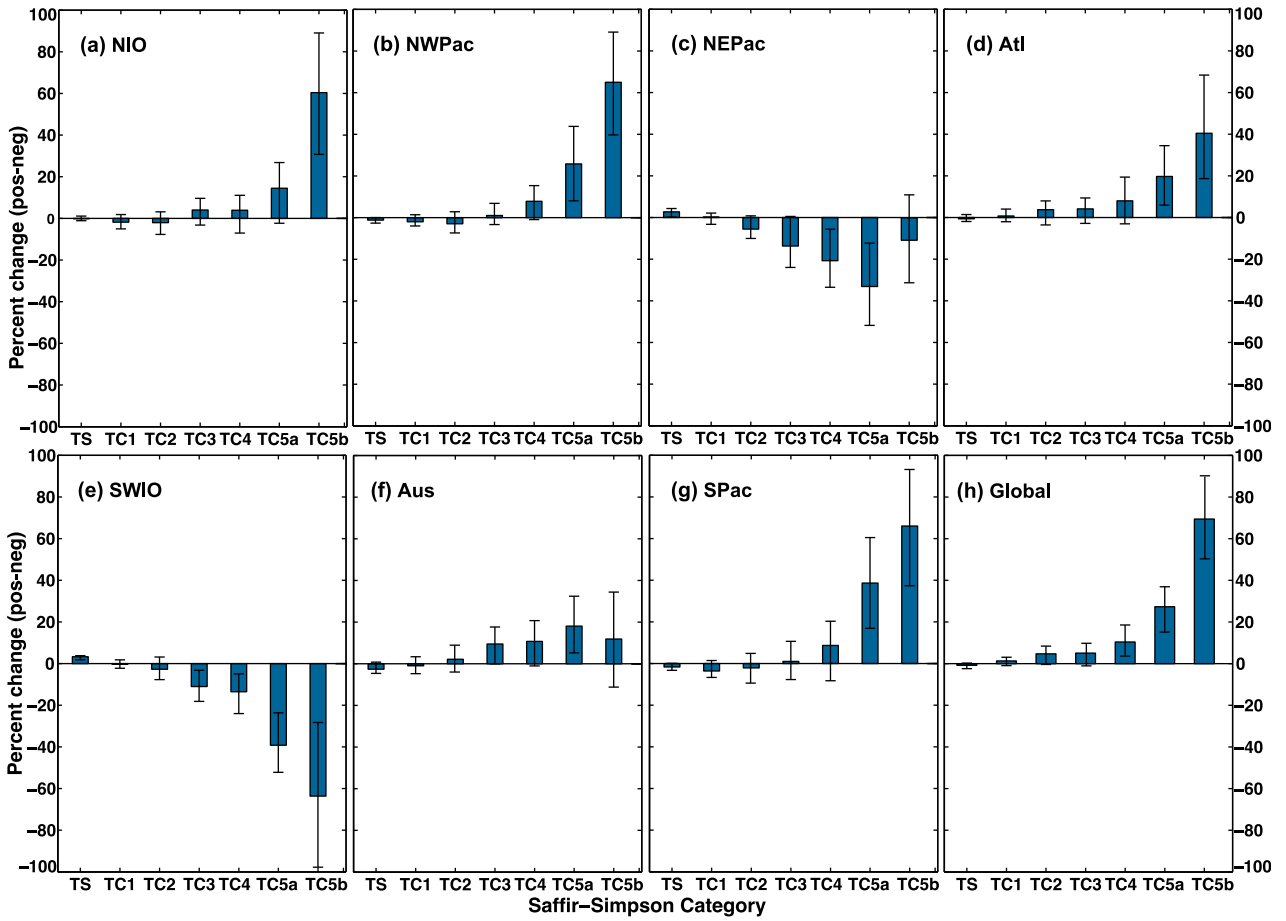

Figure 9. Histogram of relative anomalies in the intensity distribution of TCs in each basin (in % difference of TC-days/yr between the "positive" and "negative" experiments). The last figure ("global") has been obtained by contrasting all TCs located over positive CI anomalies with their negative CI anomalies counterpart, regardless of which experiment ("positive" or "negative") they belong to. Error bars show the 90% confidence interval from a bootstrap calculation taking each of the 30 simulated years as an independent event.

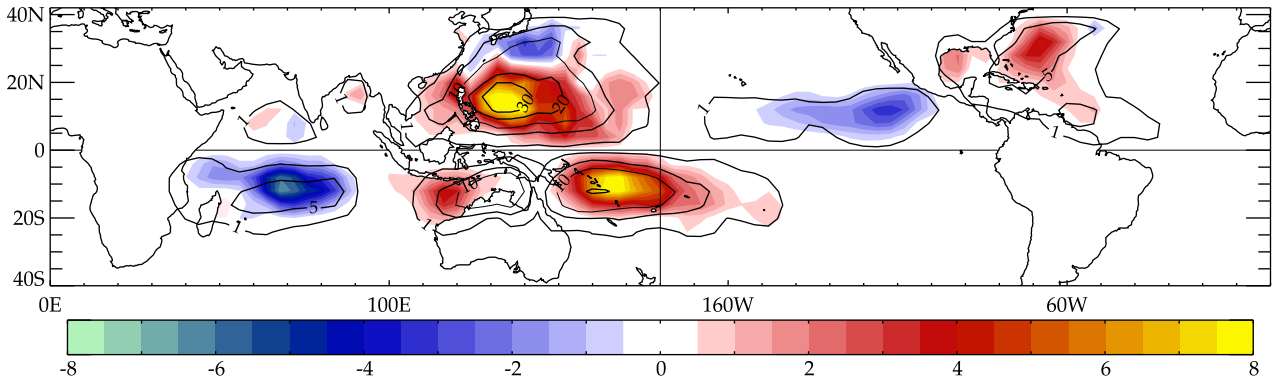

Figure 10. Map of Category 5 TCs number (black contours) and anomalies between "positive" and "negative" years (shading; in 10^{-3} TCs per year and per $1° \times 1°$ lon-lat box).

We further divide the fifth category into two subcategories (as defined in section 2.1) to highlight the higher sensitivity of the most extreme storms to ocean conditions. Within the Category 5, TCs with the strongest winds ("5b" category) are usually most sensitive to interannual variations of the ocean stratification, with the exception of the Aus and NEPac basins. The modulation of the frequency of these extremely intense TCs by oceanic stratification variability reaches 60% in the Indian Ocean and West Pacific basins. Figure 9h summarizes these observations by merging TCs simulated in all basins in two groups: TCs located over positive CI anomalies ("favorable" conditions) in one group and their counterparts in the other simulations that are located over negative CI anomalies ("unfavorable" conditions) in a second group. Natural interannual variability of ocean stratification at a given location alters TCs occurrence by 10%, 28%, and 69% for Category 4, 5a, and 5b TCs, respectively.

Figure 10 further provides a geographical view of how Category 5 TC occurrence is altered between the "positive" and "negative" experiments. The mean geography of modeled Category 5 occurrence is realistic in the SWIO, BoB, and Pacific basins but Category 5 frequency is overestimated in the Arabian Sea, underestimated in the Caribbean Sea, and shifted eastward in the "Aus" region. Largest changes in TC Category 5 occurrence are found in the West Pacific: off the coasts of Philippines in the northern hemisphere and in the Solomon-Vanuatu-Fiji region in the southern hemisphere. The southwestern Indian Ocean, south of the thermocline ridge region, also exhibits important changes in Category 5 counts. There is a significant relative anomaly of Category 5 TCs in the northern Bay of Bengal, along the coasts of Bangladesh and Myanmar. In the NEPac, TC Category 5 counts are altered by ocean conditions in a 8–16°N band and off the coast of Mexico. TC Category 5 frequency is also modulated by ocean stratification between north-western Australia and southern Indonesian islands. Finally, we observe a large modulation of Category 5 TCs north of Cuba and east of Florida, but we should take this result with caution given that the modeled Category 5 frequency is overestimated in this region (not shown).

To place the ocean stratification influence on TCs in context, Appendix A shows how atmospheric and sea surface temperature variability associated with El Niño influences TC activity. Appendix A shows that the SST and atmospheric interannual variability (vorticity, shear, tropospheric moisture...) has a greater impact on TC activity than oceanic subsurface stratification; however, when focusing on the most intense TCs, the upper ocean stratification influence on TCs numbers is of the same order of magnitude.

5.3. Relation Between the Strongest TCs and Ocean Stratification

We have seen that upper ocean stratification variability influences the strongest TCs most. This subsection discusses how the occurrence of the most intense TCs can be related to ocean subsurface variability.

We mentioned earlier that all TCs display the same sensitivity of their intensification rate to the surface cooling they induce. The higher sensitivity of Category 5 TCs to interannual CI variability is hence related to the fact that the surface cooling they induce is more sensitive to subsurface thermal stratification. Category 5 TCs are usually associated with WPi values of 4 or higher [*Vincent et al.*, 2012b, Figure 4b]. Their surface cooling is hence highly sensitive to upper ocean stratification (Figure 5). Changing ocean stratification from $CI = 10$ to $CI = 30$ $(J\ m^{-2})^{1/3}$ results in a decrease of the mean surface cooling from -2.5 to $-0.5°C$ for

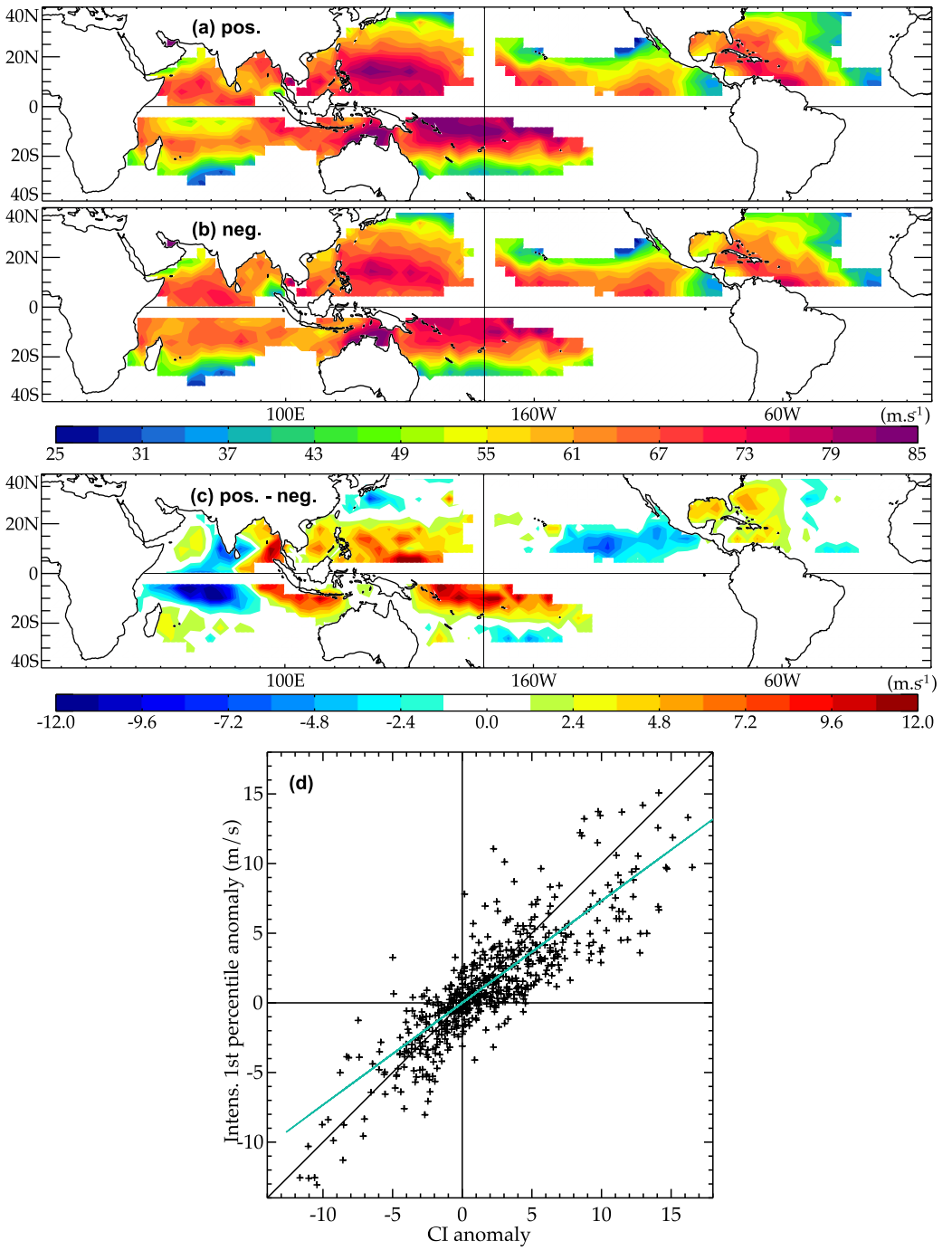

Figure 11. Map of the highest percentile cyclone intensity in each 4° × 4° lon-lat region for (a) "positive," (b) "negative," (c) "positive"-"negative" experiments, and (d) scatterplot of the highest percentile cyclone intensity anomalies versus CI interannual anomalies at each location (blue line is the linear fit with slope 0.8 m s^{-1}/CI unit).

WPi = 4, but changes it by less than 0.5°C for TCs with WPi under 2 (Figure 5a). This partly explains why intense TCs are more affected by ocean stratification variability. Physically, intense TCs can trigger deeper mixing and thus be sensitive to temperatures well below the ML. Another part of the explanation is related to the fact that the most intense TCs need more time to reach their maximum intensity, and increased surface cooling slows their intensification, preventing them from reaching higher intensity. As a result, there is a relation between the most intense storms and upper ocean stratification. Figures 11a and 11b show maps of the highest percentile of TC wind speed found at each location in the two experiments. Figure 11c shows that upper ocean stratification interannual variability modifies the intensity of the most intense storms that

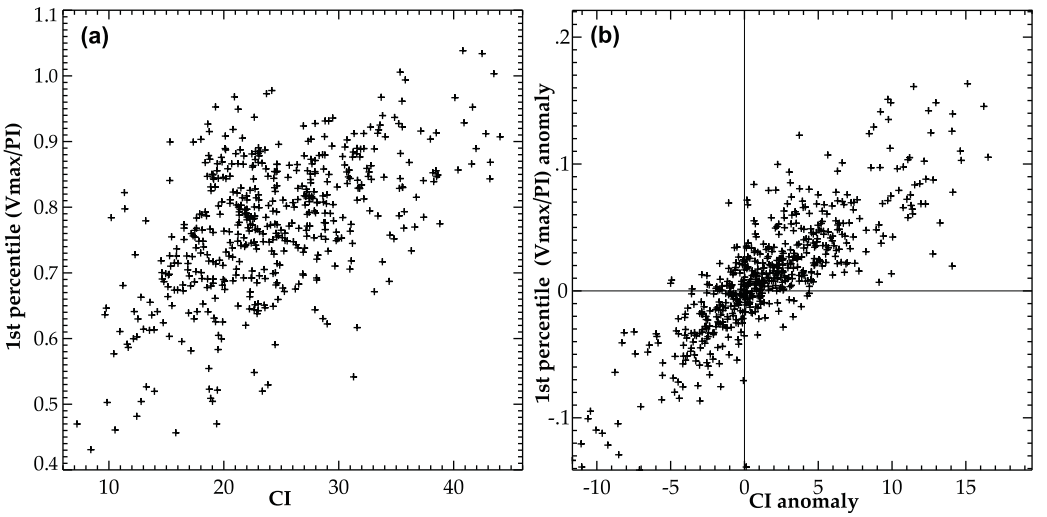

Figure 12. (a) Intensity of the highest percentile TC wind normalized by its PI (at the time the TC reached its maximum intensity) as a function of CI under the TC; (b) same as Figure 12a but for the anomalies between the two experiments. Values are calculated in each 4° × 4° lon-lat boxes over the ocean and within the 30°S–30°N latitude band.

can be expected at a given location. The sensitivity of the storm intensity highest percentile to interannual CI variations is ∼0.8 m s^{-1}/CI unit (Figure 11d). Typical variations of CI by a value of 10 units between two different TC-seasons will result in a 8 m s^{-1} (15 kt) change in the maximum winds of the most intense storms.

The most intense storm that can be sustained at a given place can be estimated from the PI value [*Emanuel*, 1999]. It is well known that vertical tropospheric wind shear is a major constraint that prevents TCs from reaching their PI [*Tang and Emanuel*, 2010]. Upper ocean stratification also plays a role in limiting the maximum intensity of TCs as suggested by *Lin et al*. [2013]. Figure 12a indeed shows that high CIs tend to be associated with intense storms that get closer to their potential intensity. Unfavorable subsurface thermal stratification can hence be seen as an additional constraint on TC maximum intensity. Anomalies in the intensity of the strongest storms normalized by their PI vary linearly with interannual anomalies of ocean stratification (Figure 12b).

6. Conclusion

6.1. Summary

The intensity of a tropical cyclone (TC) depends on its large-scale atmospheric environment [e.g., *Emanuel et al*., 2004]. TC intensity is hence modulated by climate variability. Many studies have shown how climatic variations of the atmospheric environment (shear, vorticity, midtropospheric humidity...) modulate TC activity. More recently, several observation-based studies have suggested that the ocean subsurface interannual variability may also exert an influence on TCs activity [*Xie et al*., 2002; *Wada and Chan*, 2008; *Balaguru et al*., 2013]. Coupled climatic modes—such as ENSO—induce environmental changes in both the ocean and atmosphere. It is hence difficult to disentangle the respective influences of the ocean and the atmosphere on TC activity in observational studies. Here we use the *Emanuel* [2006] downscaling approach that allows simulating a large number of TCs on the full extent of the intensity distribution, including the most intense TCs. This approach allows us to isolate the effects of the upper ocean stratification variability on TCs from those of the atmosphere and sea surface temperature. We performed two experiments for each basin, which differ only by the subsurface thermal stratification. The upper ocean thermal stratification difference between the two experiments is representative of the main mode of the upper ocean stratification variability in each TC basin.

This variability is largely driven by ENSO in the Pacific Ocean and correlated to both ENSO and the IOD in the Indian Ocean. Its amplitude is particularly large in the Western and North-eastern Tropical Pacific and in the Thermocline Ridge of the Indian Ocean (TRIO) region. This interannual variability of upper ocean

stratification influences the integrated TC activity as measured by the power dissipated (PD) by TCs by about 10% in all basins, but regional changes can be larger, as in the TRIO region where PD changes by up to 50%.

Ocean stratification variability mostly influences the occurrence of strongest TCs, accounting for ∼30% change in Category 5 TCs number at global scale and up to 40% in the southern Indian Ocean and southwestern Pacific Ocean. Within Category 5, the most intense TCs (winds greater than 85 m s^{-1}) are even more heavily affected, with basin-wide TC-days changing by about 70%. Although interannual variations of ocean stratification only marginally affect weaker storms (categories lower than 4), this does not imply that these TCs are not affected by air-sea interactions, but that the ocean feedback does not exhibit large interannual variations.

Subsurface ocean properties influence TCs through their control of the TC-induced surface cooling. This surface cooling increases with TC power at a rate that grows as the mixed layer becomes thinner and the thermal stratification below becomes tighter. The strong sensitivity of the most intense TCs to upper ocean stratification variability can thus be related to the stronger sensitivity of the surface cooling they induce to upper ocean stratification. Our results indeed show that the ratio of the intensity of most intense TCs to their potential intensity (PI) can be related to ocean stratification interannual variability. Increased cooling due to lower cooling inhibition (CI) slows down TC intensification rates, preventing them from reaching their potential intensity. A shallow mixed layer and/or highly stratified thermocline can thus be seen as an additional constraint to those from atmospheric background properties (e.g., vertical shear) on TC maximum potential intensity. Although atmospheric variability has a greater impact on overall TC activity, we show that oceanic stratification variability also significantly influences the most intense TCs.

6.2. Limitations and Perspectives

Due to its modest numerical cost, our modeling framework allows simulating tens of thousands of TCs including the most intense cyclones. While this allows us to identify the influence of ocean stratification variability on intense cyclones, applying such an approach to observational data proves difficult, as we only sample a few Category 5 TCs every year. The simplicity of our ocean-atmosphere modeling framework is also not able to account for the full range of processes involved in the TC intensification. On the atmospheric side, the axisymmetric TC model we use accounts indirectly (via a parameterization) for the 3-D processes—such as vertical wind shear—that influence TC intensity. In the ocean, the one-dimensional ocean model used only accounts for vertical mixing processes. *Yablonsky and Ginis* [2009] have shown that vertical advection significantly contributes to the surface cooling associated with slow-moving TCs. In this case, TCs should be more sensitive to subsurface thermal conditions than our estimation. Using more complex coupled atmospheric and oceanic general circulation models (CGCMs) may help to improve the quantitative assessment of the influence of upper ocean stratification variability on TCs intensification. However, using CGCMs considerably increase the computational cost of such experiments and usually prevents one from studying the strongest TCs as these models have a too coarse resolution (typically up to 20 km) [e.g., *Murakami and Wang*, 2010] and do not produce as intense TCs as observed [e.g., *Gentry and Lackmann*, 2010].

Another limitation of our approach is that it only accounts for part of the thermal stratification variability. We indeed use the first EOF mode to describe the stratification variability in each basin. While this is a good summary of the total interannual variability in the West Pacific and Indian Ocean basins, the Atlantic and Northeast Pacific deserve further investigation as the first EOF in these basin only explains a limited fraction of the total variance (Table 1). In addition, we did not account for interannual variability of the haline stratification. While this is usually of second order as compared to thermal stratification, local studies in the BoB [e.g., *Neetu et al*., 2012] or the Amazon river plume [*Balaguru et al*., 2012] suggest that salinity stratification may play a significant role regionally. In addition, we only assess the influence of large-scale interannual oceanic variations. Our approach hence does not account for the effects of oceanic stratification variability in TC regions with large eddy variability, such as the Gulf of Mexico or the Kuroshio region. Similarly, this paper did not address the upper ocean stratification changes associated with natural decadal/multidecadal fluctuations and climate change. The impact of subseasonal and long-term upper ocean variations on TCs intensification therefore deserves further investigation.

These results have practical consequences regarding TCs statistical and dynamical forecasting. As the intensity of weak TCs (Category 3 or less) are only marginally affected by interannual ocean stratification

changes, it is a reasonable approximation to use climatological temperature and salinity ocean profiles to account for the ocean feedback on these TCs. Accounting for ocean stratification climatic variability could, however, improve the forecast accuracy for intense TCs, which are responsible for large societal damages and are significantly affected by interannual ocean stratification changes.

Appendix A: Discussion on the Significance of Oceanic Versus Atmospheric Control of TC Activity

This paper assesses the influence of *oceanic* thermal stratification variability on TCs, in relation to dominant modes of tropical climate variability. Coupled tropical modes of variability (such as ENSO) also alter the *atmospheric* environment that influences TCs activity. To provide a rough quantification of the respective influence of changes in large-scale atmospheric environment against subsurface oceanic variations, Figure A1 displays the differences in TC intensity distribution in response to atmospheric parameters and SST changes related to ENSO. The simulation presented here uses an unvarying ocean thermal stratification and thus accounts solely for the effects of SST, midtropospheric humidity, upper troposphere temperature, and vertical wind shear interannual variability. El Niño and La Niña periods have been selected here using a similar strategy as for oceanic conditions but based on 10% highest (El Niño) and lowest (La Niña) percentile months of the Niño 3.4 index time series (see section 3.3). Results for "La Niña minus El Niño" are displayed in Figure A1 and Table 3 to ease comparison with Figure 9 as the first CI EOF in the Indo-Pacific basins are negatively correlated to ENSO (Table 2).

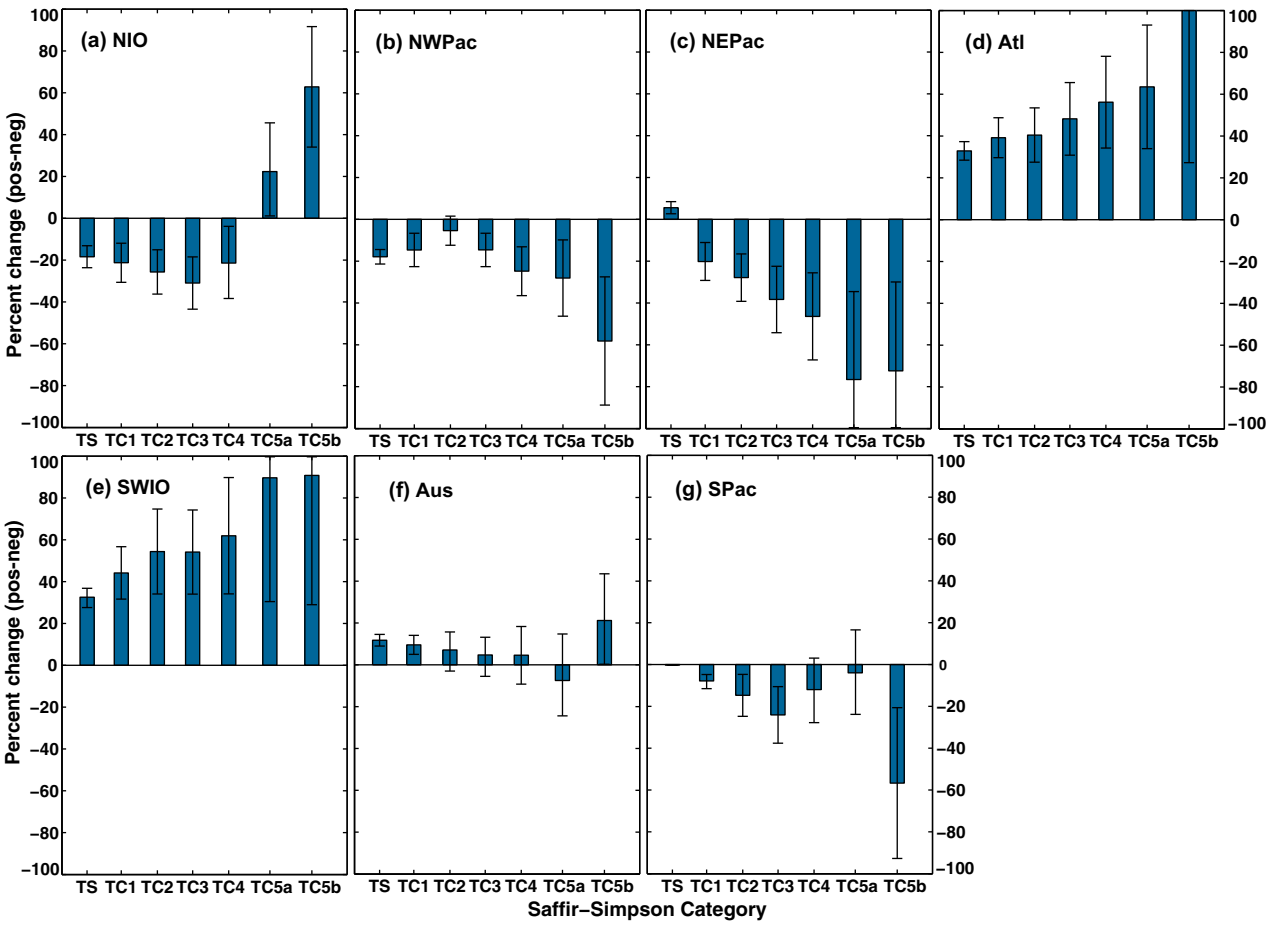

Figure A1. Same as Figure 9 but for the difference between La Niña and El Niño TC-seasons in each basin.

The largest atmospheric influence is found in the southwestern Indian Ocean, Northeast Pacific, and Atlantic basins, with an integrated TC activity change (measured through PD) of ∼60–80% in these basins, 5–10 times larger than the subsurface oceanic influence (Table 3). In the South Pacific and north Australian shelf, atmospheric related changes reach 10–15%, a similar order of magnitude as the upper ocean stratification influence (Table 3). Interannual variability of the upper ocean stratification in all basins except the Atlantic is to a large extent driven by ENSO (i.e., these basins display a significant correlation between the first principal component of CI and Nino34 index are correlated). For these basins, comparing Figure 9 and Figure A1 roughly quantify the respective influence of the changes in ocean subsurface and atmospheric environment associated with ENSO on TC count as a function of TC category. The most striking difference between these two figures is the significant influence of atmospheric variability for all TCs categories, while ocean subsurface only alter the strongest storms. However, when focusing on Category 5 TCs, the ocean subsurface and atmospheric influences on TC-days is qualitatively similar for the Indian Ocean and Western Pacific, while the atmospheric control dominates changes in Category 5 TCs-days for the Atlantic and Northeast Pacific. In the southwestern Indian Ocean and Western Pacific, oceanic subsurface and atmospheric have opposite influences on TC-days, each contributing to ∼40%. In the NIO, La Niña (and/or negative IOD) oceanic and atmospheric signatures both contribute to favor the occurrence of extreme TCs.

This analysis therefore reveals that, while SST and atmospheric interannual variability have a greater impact than oceanic subsurface stratification for TCs below Category 4, those two effects are of the same order for most intense TCs.

Acknowledgments

Results presented in this paper were generated using MyOcean products. We thank the Mercator team for providing us access to the GLORYS2 ocean reanalysis data. TC data from the Joint Typhoon Warning Center (JTWC) database are available at ftp://texmex.mit.edu/pub/emanuel/HURR/tracks_netcdf. E.M. Vincent was supported by the NOAA Climate and Global Change Postdoctoral Fellowship Program, administered by the University Corporation for Atmospheric Research. M. Lengaigne and J. Vialard were supported by the IFCPAR (Indo-French Centre for Promotion of Advanced Research, New Delhi) 4907-1 proposal.

References

Aparna, S. G., J. P. McCreary, D. Shankar, and P. N. Vinayachandran (2012), Signatures of Indian Ocean Dipole and El Niño–Southern Oscillation events in sea level variations in the Bay of Bengal, *J. Geophys. Res.*, *117*, C10012, doi:10.1029/2012JC008055.

Balaguru, K., P. Chang, R. Saravanan, L. R. Leung, Z. Xu, M. Li, and J.-S. Hsieh (2012), Ocean barrier layers' effect on tropical cyclone intensification, *Proc. Natl. Acad. Sci. U. S. A.*, *109*(36), 14,343–14,347.

Balaguru, K., L. Ruby Leung, and J.-H. Yoon (2013), Oceanic control of Northeast Pacific hurricane activity at interannual timescales, *Environ. Res. Lett.*, *8*(4), 044009, doi:10.1088/1748-9326/8/4/044009.

Boulanger, J.-P., and C. Menkes (1995), Propagation and reflection of long equatorial waves in the Pacific Ocean during the 1992–1993 El Niño, *J. Geophys. Res.*, *100*(C12), 25,041–25,059, doi:10.1029/95JC02956.

Chiang, J. C., and D. J. Vimont (2004), Analogous Pacific and Atlantic meridional modes of tropical atmosphere-ocean variability, *J. Clim.*, *17*(21), 4143–4158.

Chu, P.-S. (2004), ENSO and tropical cyclone activity, in *Hurricanes and Typhoons: Past, Present, and Potential*, pp. 297–332, Columbia Univ. Press, New York.

Cione, J. J., and E. W. Uhlhorn (2003), Sea surface temperature variability in hurricanes: Implications with respect to intensity change, *Mon. Weather Rev.*, *131*(8), 1783–1796.

Deser, C., M. A. Alexander, S.-P. Xie, and A. S. Phillips (2010), Sea Surface Temperature Variability: Patterns and mechanisms, *Annu. Rev. Mar. Sci.*, *2*(1), 115–143, doi:10.1146/annurev-marine-120408-151453.

Emanuel, K. A. (1986), An air-sea interaction theory for tropical cyclones. Part I: Steady-state maintenance, *J. Atmos. Sci.*, *43*(6), 585–605.

Emanuel, K. A. (1999), Thermodynamic control of hurricane intensity, *Nature*, *401*, 665–669.

Emanuel, K. A. (2005), Increasing destructiveness of tropical cyclones over the past 30 years, *Nature*, *436*(7051), 686–688, doi:10.1038/nature03906.

Emanuel, K. A. (2006), Climate and tropical cyclone activity: A new model downscaling approach, *J. Clim.*, *19*(19), 4797–4802.

Emanuel, K. A., C. DesAutels, C. Holloway, and R. Korty (2004), Environmental control of tropical cyclone intensity, *J. Atmos. Sci.*, *61*(7), 843–858, doi:10.1175/1520-0469(2004)061<0843:ECOTCI>2.0.CO;2.

Emanuel, K. A., S. Ravela, E. Vivant, and C. Risi (2006), A statistical deterministic approach to hurricane risk assessment, *Bull. Am. Meteorol. Soc.*, *87*(3), 299–314.

Emanuel, K. A., R. Sundararajan, and J. Williams (2008), Hurricanes and global warming: Results from downscaling IPCC AR4 simulations, *Bull. Am. Meteorol. Soc.*, *89*(3), 347–367, doi:10.1175/BAMS-89-3-347.

Ferry, N., et al. (2012), GLORYS2V1 global ocean reanalysis of the Altimetric Era (1993–2009) at meso scale, *Mercator Ocean Q. Newsl.*, *44*, 28–39.

Gentry, M. S., and G. M. Lackmann (2010), Sensitivity of simulated tropical cyclone structure and intensity to horizontal resolution, *Mon. Weather Rev.*, *138*(3), 688–704.

Jacob, S. D., and L. K. Shay (2003), The role of oceanic mesoscale features on the tropical cyclone-induced mixed layer response: A case study, *J. Phys. Oceanogr.*, *33*(4), 649–676.

Jourdain, N. C., P. Marchesiello, C. E. Menkes, J. Lefèvre, E. M. Vincent, M. Lengaigne, and F. Chauvin (2011), Mesoscale simulation of tropical cyclones in the South Pacific: Climatology and interannual variability, *J. Clim.*, *24*(1), 3–25, doi:10.1175/2010JCLI3559.1.

Jourdain, N. C., M. Lengaigne, J. Vialard, G. Madec, C. E. Menkes, E. M. Vincent, S. Jullien, and B. Barnier (2013), Observation-based estimates of surface cooling inhibition by heavy rainfall under tropical cyclones, *J. Phys. Oceanogr.*, *43*(1), 205–221, doi:10.1175/JPO-D-12-085.1.

Jourdain, N. C., B. Barnier, N. Ferry, J. Vialard, C. E. Menkes, M. Lengaigne, and L. Parent (2014), Tropical cyclones in two atmospheric (re)analyses and their response in two oceanic reanalyses, *Ocean Modell.*, *73*(C), 108–122, doi:10.1016/j.ocemod.2013.10.007.

Kalnay, E., et al. (1996), The NCEP/NCAR 40-Year Reanalysis Project, *Bull. Am. Meteorol. Soc.*, *77*, 437–471.

Kossin, J. P., and D. J. Vimont (2007), A more general framework for understanding Atlantic hurricane variability and trends, *Bull. Am. Meteorol. Soc.*, *88*(11), 1767–1781, doi:10.1175/BAMS-88-11-1767.

Lin, I.-I., C.-C. Wu, I.-F. Pun, and D.-S. Ko (2008), Upper-ocean thermal structure and the Western North Pacific category 5 typhoons. Part I: Ocean features and the category 5 typhoons' intensification, *Mon. Weather Rev.*, *136*(9), 3288–3306, doi:10.1175/2008MWR2277.1.
Lin, I.-I., P. Black, J. F. Price, C. Y. Yang, S. S. Chen, C. C. Lien, P. Harr, N. H. Chi, C. C. Wu, and E. A. D'Asaro (2013), An ocean coupling potential intensity index for tropical cyclones, *Geophys. Res. Lett.*, *40*, 1878–1882, doi:10.1002/grl.50091.
Lloyd, I. D., and G. A. Vecchi (2011), Observational evidence for oceanic controls on hurricane intensity, *J. Clim.*, *24*(4), 1138–1153, doi:10.1175/2010JCLI3763.1.
Madec, G. (2008), NEMO ocean engine, in *Note du Pôle de Modélisation*, vol. *27*, 337 pp., Inst. Pierre-Simon Laplace, Paris.
Mei, W., C. Pasquero, and F. Primeau (2012), The effect of translation speed upon the intensity of tropical cyclones over the tropical ocean, *Geophys. Res. Lett.*, *39*, L07801, doi:10.1029/2011GL050765.
Menkes, C. E., M. Lengaigne, P. Marchesiello, N. C. Jourdain, E. M. Vincent, J. Lefèvre, F. Chauvin, and J.-F. Royer (2011), Comparison of tropical cyclogenesis indices on seasonal to interannual timescales, *Clim. Dyn.*, *38*(1–2), 301–321, doi:10.1007/s00382-011-1126-x.
Murakami, H., and B. Wang (2010), Future change of North Atlantic tropical cyclone tracks: Projection by a 20-km-mesh global atmospheric model, *J. Clim.*, *23*(10), 2699–2721.
Neetu, S., M. Lengaigne, E. M. Vincent, J. Vialard, G. Madec, G. Samson, M. R. Ramesh Kumar, and F. Durand (2012), Influence of upper-ocean stratification on tropical cyclone-induced surface cooling in the Bay of Bengal, *J. Geophys. Res.*, *117*, C12020, doi:10.1029/2012JC008433.
Pielke, R. A., Jr., and C. W. Landsea (1998), Normalized hurricane damages in the United States: 1925-95, *Weather Forecasting*, *13*(3), 621–631.
Price, J. F. (1981), Upper ocean response to a hurricane, *J. Phys. Oceanogr.*, *11*(2), 153–175.
Price, J. F. (2009), Metrics of hurricane-ocean interaction: Vertically-integrated or vertically-averaged ocean temperature?, *Ocean Sci.*, *5*, 351–368.
Reyment, R. A., and K. G. Jörekog (1993), *Applied Factor Analysis in the Earth Sciences*, 2nd ed., Cambridge Univ. Press, London.
Saji, N. H., B. N. Goswami, P. N. Vinayachandran, and T. Yamagata (1999), A dipole mode in the tropical Indian Ocean, *Nature*, *401*(6751), 360–363.
Schade, L. R., and K. A. Emanuel (1999), The ocean's effect on the intensity of tropical cyclones: Results from a simple coupled atmosphere-ocean model, *J. Atmos. Sci.*, *56*(4), 642–651.
Tang, B., and K. Emanuel (2010), Midlevel ventilation's constraint on tropical cyclone intensity, *J. Atmos. Sci.*, *67*(6), 1817–1830, doi:10.1175/2010JAS3318.1.
Tang, B. H., and J. D. Neelin (2004), ENSO influence on Atlantic hurricanes via tropospheric warming, *Geophys. Res. Lett.*, *31*, L24204, doi:10.1029/2004GL021072.
Tozuka, T., T. Yokoi, and T. Yamagata (2010), A modeling study of interannual variations of the Seychelles Dome, *J. Geophys. Res.*, *115*, C04005, doi:10.1029/2009JC005547.
Vecchi, G. A., K. L. Swanson, and B. J. Soden (2008), Whither hurricane activity, *Science*, *322*(5902), 687–689.
Vialard, J., et al. (2009), Cirene: Air sea interactions in the Seychelles-Chagos thermocline ridge region, *Bull. Am. Meteorol. Soc.*, *90*, 45–61, doi:10.1175/2008BAMS2499.1.
Vincent, E. M. (2011), Interactions between Tropical Cyclones and the Ocean: Linking event scale processes to climate scale consequences, PhD thesis, Univ. Pierre et Marie Curie, Paris, doi:10.6084/m9.figshare.966608.
Vincent, E. M., M. Lengaigne, C. E. Menkes, N. C. Jourdain, P. Marchesiello, and G. Madec (2011), Interannual variability of the South Pacific Convergence Zone and implications for tropical cyclone genesis, *Clim. Dyn.*, *36*(9–10), 1881–1896, doi:10.1007/s00382-009-0716-3.
Vincent, E. M., M. Lengaigne, G. Madec, J. Vialard, G. Samson, N. C. Jourdain, C. E. Menkes, and S. Jullien (2012a), Processes setting the characteristics of sea surface cooling induced by tropical cyclones, *J. Geophys. Res.*, *117*, C02020, doi:10.1029/2011JC007396.
Vincent, E. M., M. Lengaigne, J. Vialard, G. Madec, N. C. Jourdain, and S. Masson (2012b), Assessing the oceanic control on the amplitude of sea surface cooling induced by tropical cyclones, *J. Geophys. Res.*, *117*, C05023, doi:10.1029/2011JC007705.
Wada, A., and J. C. L. Chan (2008), Relationship between typhoon activity and upper ocean heat content, *Geophys. Res. Lett.*, *35*, L17603, doi:10.1029/2008GL035129.
Webster, P. J., A. Moore, J. Loschnigg, and M. Leban (1999), Coupled dynamics in the Indian Ocean during 1997–1998, *Nature*, *401*, 356–360.
Wentz, F. J., C. Gentemann, D. Smith, and D. Chelton (2000), Satellite measurements of sea surface temperature through clouds, *Science*, *288*(5467), 847–850, doi:10.1126/science.288.5467.847.
Xie, S.-P., H. Annamalai, F. A. Schott, and J. P. McCreary Jr. (2002), Structure and mechanisms of south Indian Ocean climate variability, *J. Clim.*, *15*(8), 864–878.
Yablonsky, R. M., and I. Ginis (2009), Limitation of one-dimensional ocean models for coupled hurricane–Ocean model forecasts, *Mon. Weather Rev.*, *137*(12), 4410–4419, doi:10.1175/2009MWR2863.1.
Yu, W., B. Xiang, L. Liu, and N. Liu (2005), Understanding the origins of interannual thermocline variations in the tropical Indian Ocean, *Geophys. Res. Lett.*, *32*, 24706, doi:10.1029/2005GL024327.
Zhao, M., I. M. Held, S. J. Lin, and G. A. Vecchi (2009), Simulations of global hurricane climatology, interannual variability, and response to global warming using a 50-km resolution GCM, *J. Clim.*, *22*(24), 6653.